

# Wedging Leakage Flow and Its Impact on the Maximum Pressure Head of Bubble-Driven Micropumping

Ryan Lemmens<sup>1,2</sup> and Dennis Desheng Meng<sup>1,\*</sup>, member, IEEE

<sup>1</sup>Mechanical Engineering – Engineering Mechanics Department, Michigan Technological University, USA

<sup>2</sup>Physics Department, Michigan Technological University, USA

**Abstract** — This paper reports a previously overlooked mechanism that has a considerable effect to undermine bubble-driven micropumping in a square-shaped microchannel, and therefore limits the maximum achievable pressure head. Improvement of pumping performance by rounding the microchannel is thus proposed.

**Keywords** — Bubble-driven micropumping, Pressure head, Leakage flow, Capillaries

## I. INTRODUCTION

Bubble-driven liquid pumping in microchannels has been proven feasible and advantageous for many applications, including micro total analysis systems [1, 2], microelectronic cooling [3], and chemical micro-reactors such as micro direct methanol fuel cells ( $\mu$ DMFCs) [4, 5]. By replacing mechanical moving parts with transient gas bubbles, this category of micropumps have shown reduced fabrication cost and improved reliability. A majority of those micropumps employ Marangoni effects to establish a pressure difference across a gas bubble and thus induce asymmetric gas and liquid flow. However, it is usually challenging for those bubble-driven micropumps to generate a very high pressure head, which also directly limits the achievable flow rate with a certain flow resistance. The situation will deteriorate for microchannels bigger than hundreds of microns, which usually can only achieve a maximum pressure head of hundreds of Pa. The practical pressure head can even be much smaller than the theoretical prediction. For example, the theoretical pressure head of a recently reported micropump [6] is 660 Pa. However, the practical maximum pressure head was measured to be only 195 Pa. This paper is intended to identify the reason for this apparent discrepancy and suggest potential improvement. Based on the analysis of the failure mechanisms, we speculate that the shape of the flow channel may have a significant impact on the maximum pressure head. Devices are designed, built, and characterized to test the hypothesis.

## II. WORKING MECHANISM

A pumping mechanism similar to [6] has been adopted to study the maximum pressure head. This pumping mechanism has enabled an electrolysis-based micropump with ultra-high power efficiency [7] and the self-circulation of liquid fuel in a  $\mu$ DMFC with reduced packaging penalty and elimination of parasitic power consumption [4, 5].

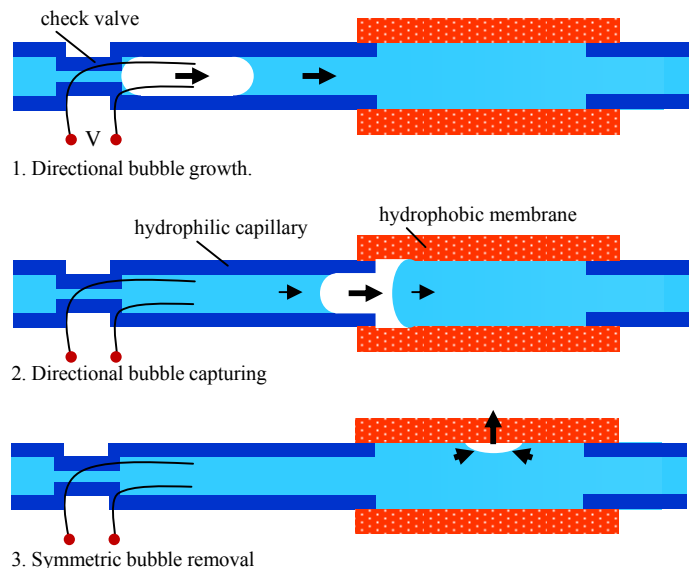


Fig. 1. Breakdown of steps for a single pumping cycle

The pumping principle is schematically shown in Fig. 1. Electrolysis of the water can be employed to generate hydrogen and oxygen gas bubbles by applying a voltage between two electrodes inserted in the flow channel. Bubble growth occurs adjacent to a portion of the channel which consists of a set of relatively narrower channels. Since larger capillary pressure can be provided by these narrower channels, the meniscus of the bubble is prevented from moving to its left, essentially acting as a check valve. This, in turn, causes asymmetric bubble growth to the rightward direction. As the meniscus of the growing bubble progresses to its right, it produces a flow of the liquid solution in the direction of its own advance. When the bubble reaches the hydrophobic nanoporous membrane, a difference in surface free energy between the bubble's menisci is introduced. As a result, the hydrophobic region pulls the bubble out of the hydrophilic region, simultaneously pulling the liquid on its left and pushing the liquid on its right, both of which induce rightward liquid pumping. The bubble is then symmetrically removed through the membrane, thus completing a single pumping cycle which produced a rightward net flow of water solution toward the outlet. Although this concept has been described with one bubble only, the existence of multiple bubbles within the flow channel is

This project has been supported by Michigan Technological University's Research Excellence Fund (Grant # R01088) along with Michigan Tech's Summer Undergraduate Research Fund (SURF).

\*Contact author: Dennis Desheng Meng, Assistant Professor, 815 R.L. Smith Building, 1400 Townsend Drive, Houghton, MI 4993, Email: [dmeng@mtu.edu](mailto:dmeng@mtu.edu), Phone: 10-906-487-3551.

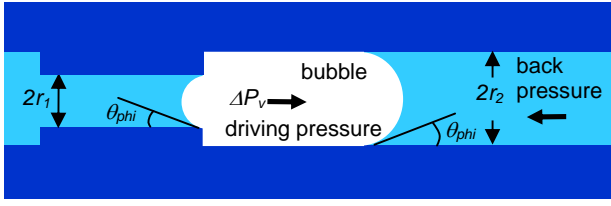


Fig. 2. Max Pressure at virtual check valve

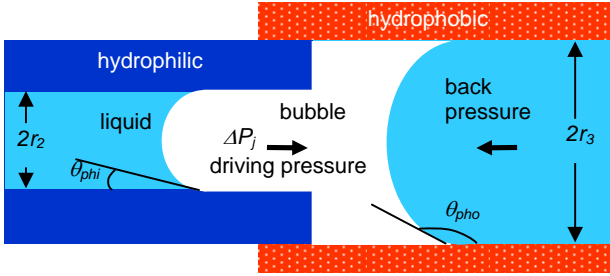


Fig. 3. Max pressure at hydrophilic / hydrophobic junction

quite frequent and does not hinder the pumping mechanism. This allows for the continuous generation of bubbles via a DC voltage across the electrodes. The pump can tolerate different rates and patterns of bubble generation as long as the venting rate is sufficiently high.

Three mechanisms or their combinations are speculated to stop the pump at a certain pressure head, as Fig.'s 2-4 illustrate. The first of these mechanisms occurs at the check valve, as Fig. 2 shows. Both capillaries are made from the same material (i.e., borosilicate glass) and therefore should exhibit the same contact angle  $\theta_{phi}$  with a given liquid. Therefore, the maximum pressure across the two menisci will be inversely proportional to their respective characteristic radii. This means that the left meniscus in Fig. 2 can tolerate a much greater pressure drop than the right one which is in a larger capillary. When a bubble is generated in the vicinity of this check valve, it will grow asymmetrically to its right. The maximum pressure difference that this check valve can withstand can be quantified as

$$\Delta P_v = 2\sigma \cos(\theta_{phi}) \cdot \left( \frac{1}{r_1} - \frac{1}{r_2} \right). \quad (1)$$

Here,  $\sigma$  is the surface tension of the solution,  $\theta_{phi}$  is the contact angle between the solution and the hydrophilic glass capillaries, and  $r_1$  and  $r_2$  are the inner radii of the valve capillary and flow capillary respectively, as denoted in Fig. 2. Failure of the check valve will occur when the back pressure (pressure head) of the flow exceeds  $\Delta P_v$ . When this occurs, the flow direction will be reversed and the bubble will be driven through the smaller capillary causing failure of the pump.

Fig. 3 illustrates the second mechanism which occurs at the junction where the channel surface changes from hydrophilic to

hydrophobic. It is similar to the first in that it deals with the particular pressure drops over the menisci involved. However, in addition to the change in characteristic diameters of the respective channel sections, the interface characteristic of the surfaces for the two menisci is also changed. The hydrophobic surface causes the contact angle to increase dramatically, essentially reversing the direction of the capillary force applied to that particular meniscus. This change in surface free energy induces a pressure difference which acts to drive the bubble rightward. This pressure difference can be quantified as

$$\Delta P_j = 2\sigma \cdot \left( \frac{\cos(\theta_{phi})}{r_2} - \frac{\cos(\theta_{pho})}{r_3} \right). \quad (2)$$

The contact angle between the solution and the hydrophobic nanoporous membrane is denoted as  $\theta_{pho}$  in (2). The outer radius of the flow capillary is denoted as  $r_3$ . Failure of the pump will occur at this junction when the back pressure (pressure head) exceeds  $\Delta P_j$ . A failure of this sort will prevent the membrane from capturing the bubble.

The third possible mechanism in accounting for the saturation of pressure head is the leakage flow in the capillaries. As Fig. 4 shows, a liquid thin film exists between the hydrophilic capillary wall [8] and the gas bubbles in gas/liquid two-phase flows [8]. For a round-shaped capillary with very slow flow (e.g., effectively static), this film tends to vanish due to the vanishing capillary number ( $Ca = \eta U_0 / \gamma$ ). However, in a square-shaped capillary, the corners will always be filled with liquid, which is known as the *wedging effect*. The liquid-filled corners form a connection between the liquid on either side of the gas bubble, disregarding  $Ca$ . When the maximum pressure head of a bubble pump is reached, the flow rate is zero. The leakage flow through the

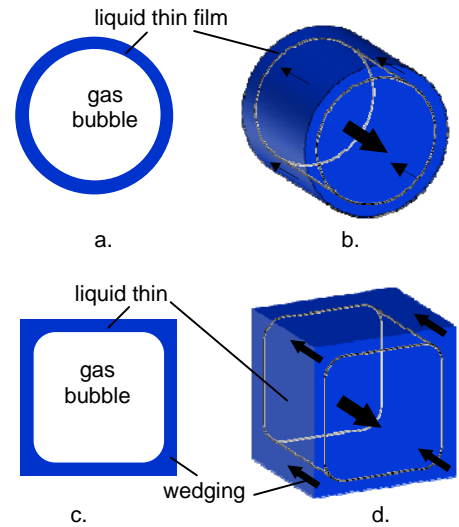


Fig. 4. The different patterns of leakage flow in a round capillary (a. and b.) or in a square capillary (c. and d.)

liquid thin film should be minimal for both round capillaries and square capillaries. However, the corner leakage for the square channel will be significant, which tends to undermine the maximum pressure head. It needs to be noted that mechanisms 1 and 2 should predict the same maximum pressure heads for round- or square-shaped capillaries with similar radii, while mechanism 3 predicts different pumping performance for the two.

As the characteristic velocity becomes non-negligible, a thin film is thought to form for both round and square shaped capillaries. This thin film forms a pathway for leakage flow. However, leakage through this thin film in most cases can be considered negligibly small when compared with that formed in a square capillary due to the wedging effect. The wedging leakage flow may still influence the pumping character significantly when the pumping rate is not zero.

### III. PUMP CONFIGURATION

In order to investigate how the pumping performance is impacted by the shape of the pump channels, an open-ended pump configuration similar to [6] is employed, as Fig. 5 illustrates.

The pumping devices are built with borosilicate glass capillaries from *Fiber Optics Inc.* These capillaries vary in size and cross sectional geometry. Both square and round capillaries are utilized as the flow channels and the valve channels. It was desired to maintain flow channels of a constant size for all pumping configurations. Therefore, a hydraulic radius of  $300\mu\text{m}$  was chosen for both the round and the square capillaries. The capillaries used for the check valves were either round with a radius of  $75\mu\text{m}$  or square with a hydraulic diameter of  $50\mu\text{m}$ . The valve itself is composed of a number of these smaller capillaries. Combinations of these sizes and shapes allowed for four different pump configurations. Platinum wire (from *A-M Systems*) with a diameter of  $50\mu\text{m}$  was used for the electrodes. A porous polypropylene membrane (from *Chemplex*) with a nominal pore radius of  $0.1\mu\text{m}$  is employed as the venting membrane. An aqueous solution of 13 wt%  $\text{Na}_2\text{SO}_4$  is used within the pump to reduce electrical resistance and therefore enhance electrolysis efficiency.

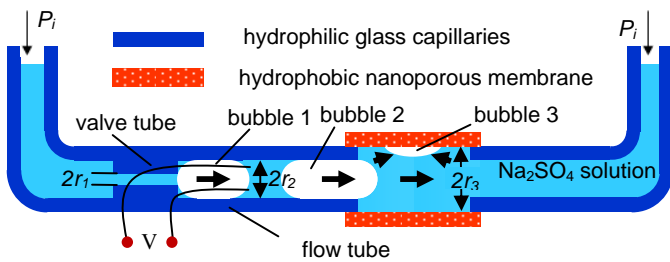


Fig. 5. Open-ended pump configuration

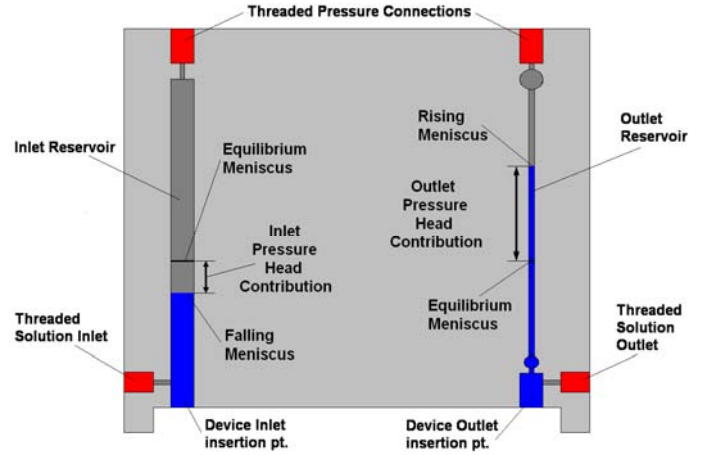


Fig. 6. Pressure chamber with description of pressure head

It is determined that the inlet and outlet of this open-ended pumping device should be slightly pressurized at the same pressure to facilitate the removal of the gas bubbles and imitate the internal pressure that would be present within a looped configuration [6]. The pressurization of the pumps inlet and outlet is achieved via a pressure chamber which is fabricated with polycarbonate and is illustrated in Fig. 6. The pressure chamber consists of an inlet and outlet reservoir to which the respective portions of the pumping device are connected. Also included are pressure connections to control the internal pressure of the chamber. All of the ports to external connections are threaded to allow for the priming and pressurization of the device prior to testing via a set of *UpChurch Scientific* tubing, fittings, and valves. Before testing, the whole chamber is pressurized to slightly above atmosphere ( $P_i = \sim 1\text{psi}$ ). The pressure is provided via a syringe which can be isolated from the system via a valve. A flow meter is incorporated into the pressurization apparatus in order to monitor pressure. The valves to these ports are closed while testing. During a test, the flow rate and pressure head can be measured by observing the rising meniscus of the outlet reservoir, the falling meniscus of the inlet reservoir, and then comparing both to their equilibrium positions.

### IV. CURRENT RESULTS

Table 1 summarizes the four micropumps we have built with capillaries of different shapes. Each pump represents a unique combination of flow and valve capillaries with different geometries. This was designed in order to show the effect that the shape of each channel type has on the characteristics of the micropumps. It is quite obvious that the geometry of the pumps has a significant impact on the measured maximum pressure head ( $\Delta P_{max}$ ). When a round flow channel is used (pumps #1 and #2), the measured maximum pressure head is much closer to the theoretical maximum ( $\Delta P_{theo}$  is the smaller of  $\Delta P_v$  and  $\Delta P_j$ ) than that measured for square flow channels (pumps #3 and #4). Hence, an increase in the practical maximum pressure head can

be achieved by simply replacing a square flow channel with a round channel. The shape of the valve channels may have an effect on the maximum pressure head as well. The notion of the existence of leakage flow in this portion of the pump is quite feasible. Similar to the flow channels, it was conjectured that the rounding of the valve channels would help to reduce the leakage flow and therefore improve the maximum achievable pressure head. This effect was found for pumps with round flow capillaries (type 1 vs. 2) while the opposite was observed for pumps with square flow capillaries (type 3 vs. 4). The wedging effect within the square flow channel is compounded by the interface of the bubble meniscus with the valve channels. It is also noticed that the size of the square- and round-shaped valve capillaries we used are not exactly the same and we have currently only conducted one set of tests for each of pump types 3 and 4. Therefore, the results for valve capillaries are not yet conclusive. More investigation is expected to reveal the impact of valve capillaries.

A representation of the relationships between the flow rate and the pressure head of the four exemplary micropumps are shown in Fig. 7. The positions of the inlet and outlet menisci were recorded by a high-performance digital camcorder during the whole pumping process for all four types of micropumps. The flow rate data can thus be collected from the video. Discrete flow rates can be found via the rising outlet meniscus as they are proportional to the meniscus velocity as well as the cross-sectional area of the outlet reservoir. The instantaneous pressure head can be determined through the height difference between the inlet and outlet reservoirs. The equilibrium menisci positions are at the same height. The initial data points for all four pumps are seen to have a significantly higher flow rate than for the rest of the data set. This dramatic difference in flow rates is due to the startup conditions of the pump. Hence, the first data point reflects only the growth rate of the first bubble within the flow channel as it progresses toward the hydrophobic membrane. Therefore, those data are discarded from Fig. 7. Upon venting of this initial bubble the pumping mechanism, as described above, is seen to take over and the pump becomes operational.

It was observed that pumps with round flow capillaries (pumps #1 and #2) produce their largest flow rates upon pump startup followed by a slow decrease in flow rate with an increase in pressure head. On the other hand, the pumps with square flow capillaries (pumps #3 and #4) produce an initial lull in flow rates.

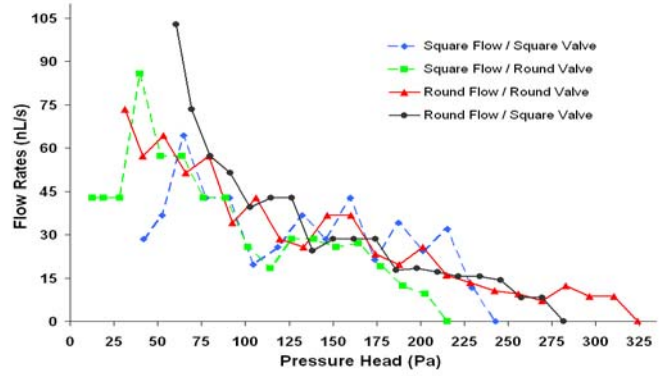


Fig. 7 Relationship between flow rates and pressure head

This lull is followed by a peak in flow rates and then a subsequent decrease as pressure head builds. The cause of the slow start up for the pumps with square flow channels is thought to be due to the initial conditions of the dynamic flow. It may take a finite amount of time for the pumping flow to establish its dominance over the leakage flow caused by the wedging effect. Further investigation is required to verify any causes of this phenomenon. It is also noticed that the flow rates of pumps with round flow capillaries are much more stable than those with square flow capillaries. For all four pumps, the flow rate slowly decreases until it becomes zero at which point the pressure head has reached a maximum.

## V. CONCLUSIONS AND FUTURE WORK

Bubble-driven micropumps with square- and round-shaped capillaries have been characterized and compared to determine the effect of the flow channel shape on micropumping performance. The achievable maximum pressure head for a pump with a square-shaped flow capillary is found to be significantly lower. This is attributed to the leakage flow through the corners. It was also observed that a more stable pumping rate can be attained through the use of round flow channels, in addition to the improvement in the maximum pressure head. Currently, most micropump configurations employ square- or rectangular shaped microchannels, which will be significantly affected by the leakage flow due to wedging effect. Round-shaped microchannels can help to increase the practical maximum pressure head as well as flow rates. Hydrogen annealing technology [9] can be employed to modify the micromachined bubble pumps and improve their performance by rounding the microchannels. Although this paper uses a specific exemplary

### 1. Key parameters and performance of pumps

Pump Type	Valve Shape	$r_1$ ( $\mu\text{m}$ )	Flow Shape	$r_2$ ( $\mu\text{m}$ )	$r_3$ ( $\mu\text{m}$ )	$\Delta P_v$ (Pa)	$\Delta P_j$ (Pa)	$\Delta P_{\text{max}}$ (Pa)	$\Delta P_{\text{theo}} / \Delta P_{\text{max}}$ (%)
1	Round	75	Round	300	420	1640	660	324	49%
2	Square	50	Round	300	420	2730	660	282	42.70%
3	Round	75	Square	300	420	1640	660	215	33%
4	Square	50	Square	300	420	2730	660	243	36.80%

pumping configuration, the conclusion should also be valid for bubble-driven micropumps with various configurations.

The effect of the shape of the valve channels on the maximum pressure head will be studied along with an investigation into the presence of leakage flow in this portion of the pump to provide for an optimal pump configuration. A further examination of the flow rate vs. pressure head relationship will also be undertaken.

#### ACKNOWLEDGMENT

The authors wish to thank Professor J. S. Allen, Professor A. Mukerjee, J. Hernandez, N. Kroodsma, M. Nie, P. Patel, and S. Santhanagopalan for their discussion and help.

#### REFERENCES

- [1] J. D. Zahn, A. deshmkh, A. P. Pisano, and D. Liepmann, "Continuous On-Chip Micropumping for Microneedle Enhanced Drug Delivery," *Biomedical Microdevices*, vol. 6, pp. 183-190, 2004.
- [2] N. R. Tas, J. W. Berenschot, T. S. J. Lammerink, M. Elwenspoek, and A. v. d. Berg, "Nanofluidic Bubble Pump Using Surface Tension Directed Gas Injection," *Analytical Chemistry*, vol. 74, pp. 2224-2228, 2001.
- [3] Y. Yokoyama, M. Takeda, T. Umemoto, and T. Ogushi, "Thermal micro pumps for a loop-type micro channel," *Sensors and Actuators A: Physical*, vol. 111, pp. 123-128, 2004.
- [4] D. D. Meng and C.-J. Kim, "A Micro Direct Methanol Fuel Cell with Self-Pumping of Liquid Fuel," in *Tech. Dig. Solid State Sensor, Actuator and Microsystems Workshop*, Hilton Head Island, 2006.
- [5] D. D. Meng and C.-J. Kim, "Embedded Self-circulation of Liquid Fuel for a Micro Direct Methanol Fuel Cell," in *Proc. IEEE Int. Conf. Micro Electro Mechanical Systems*, Kobe, Japan, 2007, pp. 85-8.
- [6] D. D. Meng and C.-J. C. Kim, "Micropumping of Liquid by Directional Growth and Selective Venting of Gas Bubbles," *Lab on a Chip*, vol. 8, pp. 958 - 968, 2008.
- [7] D. D. Meng and C.-J. Kim, "Micropumping by Directional Growth and Hydrophobic Venting of Bubbles," in *Proc. The 18th IEEE Int. Conf. on Micro Electro Mechanical Systems*, Miami, FL, 2005, pp. 423-426.
- [8] M. T. Kreutzer, F. Kapteijn, J. A. Moulijn, and J. J. Heiszwolf, "Multiphase monolith reactors: Chemical reaction engineering of segmented flow in microchannels," *Chemical Engineering Science*, vol. 60, pp. 5895-5916, 2005.
- [9] M.-C. M. Lee and M. C. Wu, "3D Silicon Transformation Using Hydrogen Annealing," in *Tech. Dig. Solid-State Sensor, Actuator and Microsystems Workshop*, Hilton Head Island, 2004, pp. 19-22.